Long-wavelength limit and Fano profiles of extraordinary transmission through metallic slit gratings in the THz range

Christophe Minot,[1,2] Yanko Todorov,[2] Damien Armand,[3] Frédéric Garet,[3] and Jean-Louis Coutaz[3]
[1]*Institut Telecom/Telecom ParisTech, 46 rue Barrault, 75634 Paris Cedex 13, France*
[2]*CNRS-Laboratoire de Photonique et de Nanostructures, Route de Nozay, 91460 Marcoussis, France*
[3]*IMEP-LAHC, UMR 5130 du CNRS, University of Savoie, 73376 Le Bourget du Lac, France*
(Received 12 August 2009; published 20 October 2009)

Transmission measurements through thin metallic slit gratings deposited over a dielectric substrate are presented in the THz range below and above the limit at which radiative diffraction occurs. The results are analyzed owing to numerical and analytical modeling based on the modal method, especially in the long-wavelength limit. Rayleigh-Wood anomalies and extraordinary transmission are observed and explained by a pure interference mechanism, which gives rise to Fano profiles at discrete mode wavelengths over a diffraction background fed by evanescent diffraction orders.

DOI: 10.1103/PhysRevB.80.153410 PACS number(s): 73.20.Mf, 41.20.Jb, 42.79.Dj, 71.36.+c

The physical origin of extraordinary transmission through subwavelength apertures in metallic films has been a matter of controversy since the effect was demonstrated with two-dimensional hole arrays at optical frequencies.[1] Early interpretations emphasized the role of electronic polarizability in the metal, which is governed by electronic conduction and the dynamics of surface plasmons.[2,3] While mixed light-matter excitations, the surface plasmon polaritons (SPPs), undoubtedly are involved under adequate polarization conditions, extraordinary transmission through periodic arrays more profoundly relies upon diffraction[4–6] and can be described within the dynamical diffraction theory.[4] The incident electromagnetic waves only interfere with discrete eigenmodes,[5,7–9] constructively at transmission maxima or destructively at transmission minima. Such eigenmodes may be SPPs,[7] or any other surface wave that may arise when dielectric layers are deposited on the grating.[8,9] Fabry-Pérot resonances in the apertures also give rise to near unity transmission,[10–12] but the line shapes do not exhibit dips at transmission minima. Recent theoretical approaches further attenuate the importance of SPPs in the mechanism of extraordinary transmission, because the SPP generation efficiency progressively diminishes as the wavelength increases.[13]

In this Brief Report, the continuum of evanescent surface waves generated by diffraction at the metal-dielectric interfaces is shown to be a key ingredient to explain extraordinary transmission, rather than the SPP concept. This is demonstrated using guided mode resonances in an underlying substrate as discrete eigenmodes. Theoretically, a fully analytical model is derived from the modal method. Experimentally, transmission measurements through a metallic grating of thin rectangular slits deposited on a highly transparent substrate are performed at THz frequencies.[14] On one hand, the one-dimensional slit array under classical incidence, i.e., with the incidence plane perpendicular to the slits, allows clear assignments to SPP effects, because excitation of surface plasmons is forbidden when the incident electric field is parallel to the metallic surfaces (TE polarization). On the other hand, it is essential to carry out measurements over a broad spectral range, both below and above the diffraction limit where the first radiative diffracted order appears, and this is most easily accomplished in the THz range, especially using broadband time-domain techniques. Furthermore, in this range, usual metals exhibit very low losses and very weakly deviate from the perfect metal. Also, surface roughness and fabrication defects can be made negligible at the wavelength scale. As a result, resonance widths and mode couplings are minimally obscured by dissipation or broadening.

The sample is made by evaporating a gold layer (thickness $h=320$ nm) over a high resistivity (8–14 kΩ cm) silicon wafer (diameter of 2″) and a thin 15 nm Ti buffer layer. Parallel metal strips are patterned thanks to standard photolithography and lift-off techniques. The slit periodicity is $d=100$ μm and the width is $a=50$ μm. After metal deposition, the substrate is thinned down to $L=143$ μm by etching its back side mechanically. The transmission spectrum is measured thanks to a classical THz time-domain setup,[14] using LTG-GaAs photoswitches as emitting and receiving antennas. The latter are excited by fs pulses at 800 nm from a mode-locked Ti:Sa laser. The THz beam is made almost parallel at the sample location by a set of parabolic mirrors (3 cm diameter at 1 THz). It is linearly polarized, with an orthogonal component less than 1%. The ultimate resolution of the setup is ~6 GHz. In practice it is only better than 10 GHz due to the finite number of illuminated slits.

Figure 1 shows THz amplitude transmission spectra for TM and TE polarizations at normal incidence. Weak transmission Rayleigh-Wood anomalies and extraordinary transmission ($>\sqrt{0.5}$, i.e., 70.7%) are observed above the diffraction limit (~0.9 THz). Below that limit, successive TM transmission peaks remain close to unity, while the TE peaks progressively increase. As expected from former results at optical frequencies, the spectra are nicely reproduced by a numerical model based on the modal method in the surface impedance approximation (see solid lines in Fig. 1), which is very satisfactory in the THz range.[14,15] Comparison with the case of an infinite substrate (dotted lines) exhibits the contribution of the grating itself, with the substrate SPP resonance in TM polarization, and brings evidence of additional substrate effects. Exact understanding of the latter and their in-

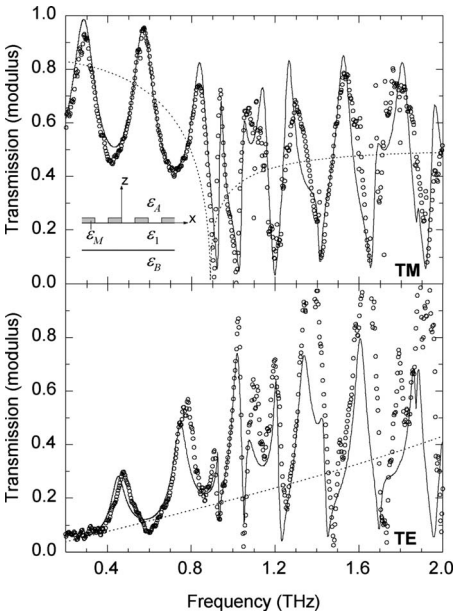

FIG. 1. THz transmission at normal incidence for TM and TE polarizations from Ref. 14: experimental data (open circles), full calculation (solid line), and calculation for infinite substrate thickness in the one-mode model (dotted line). The drawing defines the dielectric constant ε_m in each medium m.

terplay with diffraction require however more elaborate analytical derivations from Ref. 15.

At the heart of the model is the relation between the field of the incident and reflected plane waves in dielectric medium A (see drawing in Fig. 1) and the field in the slits. This relation relies upon two combined, easy to identify, and phase preserving mechanisms: (i) slit mode diffraction at both interfaces and (ii) roundtrip between the upper and lower interfaces, which gives rise to slit Fabry-Pérot effects. In the following, only the lowest slit mode is considered for either polarization, with the one-mode approximation being a very good assumption for subwavelength apertures: $a<\lambda/2$.[2,10] Then, diffraction effects are governed by the modal diffraction amplitudes,[15]

$$S_A^{\pm} = \frac{a}{2d\eta}\sum_n (1 \pm \rho_{MA}^{\pm,n})|L_n^{\pm}|^2 \equiv \frac{a}{d}\sum_n S_A^{\pm,n}, \tag{1}$$

where $\pm$ stands for TM or TE, respectively; $\eta=1/\sqrt{\varepsilon_M}$ is the surface impedance; $L_n^{\pm}$ is the modal projection of Rayleigh diffracted wave of order n; and $\rho_{MA}^{\pm,n}$ is the Fresnel reflection coefficient for this wave at a virtual plane interface between a metallic plane with surface impedance η and medium A,

$$\rho_{MA}^{+,n} = \frac{\eta\varepsilon_A - \bar{\gamma}_{An}}{\eta\varepsilon_A + \bar{\gamma}_{An}}, \quad \rho_{MA}^{-,n} = \frac{1-\eta\bar{\gamma}_{An}}{1+\eta\bar{\gamma}_{An}}, \tag{2}$$

with $\bar{\gamma}_{An}$ as the wave-vector component perpendicular to the interfaces (in reduced units of wave vector in vacuum $k_0=2\pi/\lambda$). If θ denotes the incidence angle,

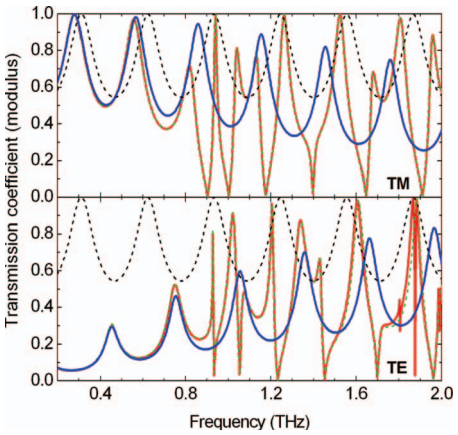

FIG. 2. (Color) THz transmission at normal incidence for TM and TE polarizations: one-mode numerical model (red curves), analytical model up to Rayleigh order $n=0$ [Eq. (5)] without (dashed black curves) and with (blue curves) evanescent cloud, or up to Rayleigh orders $n=\pm 1$ [Eq. (8), dashed green curves].

$$\bar{\gamma}_{An} = \sqrt{\varepsilon_A - (\sin\theta + n\lambda d^{-1})^2}.$$

Diffraction at the lower interface is expressed similarly using generalized reflection $R_{MB}^{\pm,n}$ or transmission $T_{MB}^{\pm,n}$ coefficients, which take into account all the interfaces between the slits and the output medium B. More specifically, in the modal diffraction amplitudes $S_B^{\pm}$, the Fresnel coefficient $\rho_{MA}^{\pm,n}$ in Eq. (1) must be replaced with $R_{MB}^{\pm,n}$, and $1\pm R_{MB}^{\pm,n}=(1\pm\rho_{M1}^{\pm,n})F_n^{\pm}$, where $F_n^{\pm}$ is a substrate Fabry-Pérot factor,

$$F_n^{\pm} = \frac{1+\rho_{1B}^{\pm,n}e^{2i\bar{\gamma}_{1n}k_0L}}{1+\rho_{M1}^{\pm,n}\rho_{1B}^{\pm,n}e^{2i\bar{\gamma}_{1n}k_0L}}. \tag{3}$$

$\rho_{1B}^{\pm,n}$ is the Fresnel coefficient at the interface between the substrate and medium B. As comparison of Fig. 1 (solid lines) to Fig. 2 (red curves) shows, the one-mode calculation retains all the essential features of the measured transmission spectra. Slight deviations are observed only near the diffraction limit or when higher-order modes are no longer subwavelength, near 2 THz.

As to the roundtrip effects, since the metal is very thin in comparison to the wavelengths, the slit Fabry-Pérot can be considered at resonance, and for a perfect metal ($\eta=0$) the transmission coefficient takes a simple form, inversely proportional to the diffraction amplitude,

$$t_0 = \frac{a}{d}\frac{\mathcal{T}_{MB}^{\pm}}{S_A^{\pm}+S_B^{\pm}}, \quad \mathcal{T}_{MB}^{\pm} = \eta^{(1\pm1)/2}T_{MB}^{\pm,0}|L_0^{\pm}|^2. \tag{4}$$

The above assumptions do not significantly alter the transmission curves (see red and green curves in Fig. 2), and Eq. (4) is retained for the rest of this Brief Report. For the sake of clarity, it is written for $\varepsilon_A=\varepsilon_B=1$.

To go further, the transmission coefficient is evaluated in the long-wavelength limit using primed variables,

$$\bar{\gamma}_{An} \simeq i|\sin\theta + n\lambda d^{-1}| \equiv \bar{\gamma}_n',$$

which amounts to setting $\varepsilon_A=0$ for order n and is valid for $n\gtrless 0$ if $|n| \gg (\sqrt{\varepsilon_A}\mp\sin\theta)d/\lambda$. When the approximation is

also legitimate at the interface with the substrate, i.e., below the diffraction limit of the structure, all the Rayleigh orders are evanescent but order zero. Then, all the evanescent orders can be summed up in Eq. (1), so that

$$S_A'^{\pm} = \frac{a}{d}\left[S_A^{\pm,0} + i\frac{\sqrt{\varepsilon_A}}{\pi}(\sqrt{\varepsilon_A}k_0 d)^{\pm 1}\mathcal{S}_\theta^{\pm}\left(\frac{a}{d}\right)\right], \tag{5}$$

where $\mathcal{S}_\theta^{\pm}(x)$ is a purely geometrical function of the aperture ratio x and the incidence angle θ, which can be given an explicit analytical form in terms of special functions for a perfect metal [otherwise, $\mathcal{S}_\theta^{\pm}(x)$ can be expanded as a power series of $\eta^{\pm 1}$]. A similar result prevails for $S_B'^{\pm}$ for the substrate is thick enough to ensure that $\varphi_n = \bar{\gamma}_{1n}k_0 L \gg 1$ and $F_n^{\pm} \simeq 1$ when $n \neq 0$. Thus, below the diffraction limit, the transmission is governed by radiative order $n=0$ together with an *evanescent cloud*, which either vanishes as or diverges as $1/k_0$ in the long-wavelength limit for TM or TE polarization, respectively. Neglecting the evanescent orders yields the black dashed curves in Fig. 2, which reflect the substrate Fabry-Pérot effects. As expected, the latter are polarization independent at normal incidence. They do not account for the slow variations of the spectra below the diffraction limit. Contrarily, the transmission is fairly accounted for by incorporating the evanescent orders (blue curves). Denoting by t_0^0 the amplitude transmission coefficient at diffraction order $n=0$ and using $\mathcal{S}=\mathcal{S}_A^{\pm}+\mathcal{S}_1^{\pm}$, where $\mathcal{S}_i^{\pm} = \sqrt{\varepsilon_i}(\sqrt{\varepsilon_i}k_0 d)^{\pm 1}\mathcal{S}_0^{\pm}/(\pi|L_0^{\pm}|^2)$ for $i=(A,1)$, the transmission $T_0^0 = |t_0^0|^2$ is not significantly altered taking $\eta=0$ in Eq. (5) and then writes

$$T_0^0 = \frac{1}{1+\mathcal{S}^2}\frac{1}{1+F(\mathcal{S})\sin^2\varphi_0 + G(\mathcal{S})\sin 2\varphi_0} \tag{6}$$

for both polarizations, with the finesse functions,

$$F(\mathcal{S}) = \frac{\mathcal{F}^2}{\pi^2}\frac{1}{\varepsilon_1}\frac{\varepsilon_1 - 1 - 4\mathcal{S}^2}{1+\mathcal{S}^2}, \quad G(\mathcal{S}) = \frac{\mathcal{F}^2}{\pi^2}\frac{1}{\sqrt{\varepsilon_1}}\frac{2\mathcal{S}}{1+\mathcal{S}^2}.$$

Hence, the substrate Fabry-Pérot behavior is roughly preserved in the long-wavelength limit, but the maximum transmission varies as $1/(1+\mathcal{S}^2)$ and the finesse of the substrate slab $\mathcal{F}=\pi\sqrt{\varepsilon_1-1}/2$ is decreased by factors $[\sqrt{(\varepsilon_1-1)/\varepsilon_1}]/2$ and $1/\sqrt{\varepsilon_1}$ as $\mathcal{S}\to 0$ and $\mathcal{S}\to\infty$ in TM and TE polarizations, respectively. In addition, the phase is shifted by $\pi/2$ in the TE polarization.

If the frequency is progressively increased, $\bar{\gamma}_{in}$ for $n\neq 0$ vanish and become real and the assumptions $\varepsilon_i \sim 0$ are no longer valid and the Rayleigh orders successively become radiative. They can be added to Eq. (5) as

$$\frac{a}{d}[S_A^{\pm,n} - S_A'^{\pm,n}], \quad \frac{a}{d}[S_B^{\pm,n} - S_B'^{\pm,n}], \tag{7}$$

where $\bar{\gamma}_{in}$ are replaced with $\bar{\gamma}_{in}'$ in Eqs. (1) and (2) to obtain $S_i'^{\pm,n}$. In $S_B^{\pm,n}$, terms such as

$$1 + R_{MB}^{+,n} = \frac{\varepsilon_1 F_n^{+}}{\eta\varepsilon_1 + \bar{\gamma}_{1n}}, \quad 1 - R_{MB}^{-,n} = \frac{\bar{\gamma}_{1n}F_n^{-}}{1+\eta\bar{\gamma}_{1n}}$$

cancel the transmission coefficient (4) at the poles of the substrate Fabry-Pérot factor $1/F_n^{\pm}=0$, i.e., when a discrete

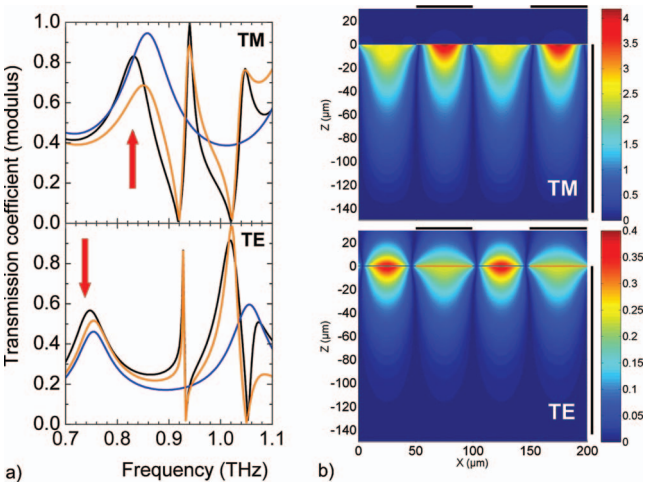

FIG. 3. (Color) (a) THz transmission at normal incidence for TM and TE polarization: full numerical model (black curves), analytical model up to Rayleigh order $n=0$ with evanescent cloud [Eq. (5), blue curves] and fitted Fano profiles (orange curves) with Fano factors $q_1^{+}=2.37$, $q_2^{+}=0.62$, $q_1^{-}=-9.98$, and $q_2^{-}=-2.36$. (b) Evanescent part of transverse field in the incidence plane, inside and above the substrate: modulus of magnetic (electric) field in TM (TE) polarization at frequencies indicated by arrows in (a). Black bars mark the extension of the substrate (right axis) and the thin metal strips at $z=0$ (top axis).

confined mode is excited by Rayleigh diffraction order n. These modes are the usual guided modes: they are radiative in the substrate plane, but evanescent in the far field in the direction perpendicular to the layers. The transmission also cancels in the TM polarization when $\eta\varepsilon_1 + \bar{\gamma}_{1n}=0$, which is the SPP resonance condition at the metal-substrate interface in the surface impedance approximation.[2] As $\eta \propto (1-i)$ is quite small in the THz range and $\bar{\gamma}_{1n}$ evolves from purely imaginary to purely real with frequency, a SPP quasiresonance occurs near $\bar{\gamma}_{1n}=0$ at the frequency of a long-wavelength surface plasmon in the metal (see dotted line for infinite substrate in Fig. 1). In the present sample, the SPP is in strong interaction with the TM substrate modes. The SPP quasiresonance is hidden but modifies the substrate mode line shapes, shifting their frequency in the vicinity of the mixed resonance condition: $(\eta\varepsilon_1 + \bar{\gamma}_{1n})/F_n^{\pm} \to 0$ at real frequencies.

Then, inserting degenerate orders $n=\pm 1$ at the metal-substrate interface, the transmission coefficient at normal incidence to the first diffraction order can be written as

$$t_0^1 = t_0^0\frac{1}{1 + 2[\mathcal{T}_{MB}^{\pm}]^{-1}[S_B^{\pm,1} - S_B'^{\pm,1}]t_0^0}. \tag{8}$$

t_0^0 is a rather slowly varying function of frequency, whereas $S_B^{\pm,1} - S_B'^{\pm,1}$ rapidly changes in the vicinity of the discrete substrate modes. Assuming that t_0^0 is a constant near a mode, T_0^1 differs from T_0^0 by a factor which tends toward 1 in the long-wavelength limit $(S_B^{\pm,1} = S_B'^{\pm,1})$, goes to zero $(S_B^{\pm,1} \to \infty)$ at the mode wavelength, and nearby reaches a maximum equal to $\sec^2 \mathrm{Arg}(t_0^0/\mathcal{T}_{MB}^{\pm})$ (≥ 1), i.e., T_0^1 exhibits all the features of a Fano profile.[5,16] Actually, Fig. 2 shows

six asymmetric lines at diffraction orders $n=\pm 1$ around the successive substrate modes. Remarkably, they are quite satisfactorily accounted for if t_0^0 is directly multiplied by appropriate Fano line shapes [see blue and orange curves in Fig. 3(a)],[17] with positive (negative) Fano factors in the TM (TE) polarization.

The evanescent Rayleigh orders can thus be considered as a *diffraction background* that strongly affects the transmission resonances above the diffraction limit and steadily persists below [see in Fig. 3(b) the transverse fields after the removal of the propagative waves, markedly localized at the metal-dielectric interfaces]. Resulting from diffraction of the incident wave, they are further rediffracted by the grating.[5,9] Together with radiative order $n=0$, they form an unstructured continuum, in which no Rayleigh diffraction anomalies appear although diffraction is taken into account to all orders in the long-wavelength limit. Above the diffraction limit, interaction of the continuum with discrete modes, such as SPPs or sub(super)strate modes, gives rise to Fano interference profiles, and the radiative diffracted orders $n\neq 0$ must be considered as deviations from the long-wavelength limit [see Eq. (7)]. They can also be viewed as order-dependent perturbations to an ideal system in which the dielectric constant of the nonmetallic layers is set to nought. Finally, as the single-particle excitations in the metal are only weakly coupled to light, the plasmons are the electronic excitations at the origin of the metal polarizability and the SPP picture,[18] but they play no specific role in the purely optical and interferential mechanisms of extraordinary transmission.

In conclusion, THz extraordinary transmission through metallic slit gratings in TM and TE polarizations relies on a Fano interference, involving interaction of discrete photonic eigenmodes with the continuum formed by the undiffracted waves and a background of diffracted waves. As evanescently confined electromagnetic energy at the metal-dielectric interface, the diffraction background can be considered as a surface mode associated with metal bulk plasmon excitations through lattice diffraction both in TM and TE polarizations. In fact, the really unique property of metallic apertures that dielectric media do not possess is their ability to reject high-order modes in the apertures thanks to metal opacity, which actually makes it possible to control subwavelength fields. No doubt, the present views also apply to two-dimensional metallic hole arrays or to any apertured conductive medium.

The authors acknowledge support by the Région Ile de France and the Conseil Général de L'Essonne, and helpful comments from F. Pardo and R. Kuszelewicz.

[1] T. W. Ebbesen, H. J. Lezec, H. F. Ghaemi, T. Thio, and P. A. Wolff, Nature (London) **391**, 667 (1998).
[2] L. Martin-Moreno, F. J. Garcia-Vidal, H. J. Lezec, K. M. Pellerin, T. Thio, J. B. Pendry, and T. W. Ebbesen, Phys. Rev. Lett. **86**, 1114 (2001); F. J. Garcia-Vidal and L. Martin-Moreno, Phys. Rev. B **66**, 155412 (2002).
[3] L. Salomon, F. Grillot, A. V. Zayats, and F. de Fornel, Phys. Rev. Lett. **86**, 1110 (2001).
[4] M. M. J. Treacy, Phys. Rev. B **66**, 195105 (2002).
[5] M. Sarrazin, J. P. Vigneron, and J. M. Vigoureux, Phys. Rev. B **67**, 085415 (2003).
[6] H. J. Lezec and T. Thio, Opt. Express **12**, 3629 (2004).
[7] D. Maystre and M. Nevière, J. Opt. **8**, 165 (1977).
[8] M. Nevière, D. Maystre, and P. Vincent, J. Opt. **8**, 231 (1977).
[9] A. Hessel and A. A. Oliner, Appl. Opt. **4**, 1275 (1965).
[10] J. A. Porto, F. J. Garcia-Vidal, and J. B. Pendry, Phys. Rev. Lett. **83**, 2845 (1999).
[11] Q. Cao and P. Lalanne, Phys. Rev. Lett. **88**, 057403 (2002).
[12] F. Marquier, J. J. Greffet, S. Collin, F. Pardo, and J. L. Pelouard, Opt. Express **13**, 70 (2005).
[13] P. Lalanne, J. P. Hugonin, and J. C. Rodier, Phys. Rev. Lett. **95**, 263902 (2005); H. Liu and P. Lalanne, Nature (London) **452**, 728 (2008).
[14] D. Armand, Y. Todorov, F. Garet, C. Minot, and J. L. Coutaz, IEEE J. Sel. Top. Quantum Electron. **14**, 513 (2008).
[15] Y. Todorov and C. Minot, J. Opt. Soc. Am. A **24**, 3100 (2007).
[16] S. Enoch, E. Popov, M. Nevière, and R. Reinisch, J. Opt. A, Pure Appl. Opt. **4**, S83 (2002).
[17] The Fano factor q characterizes the shape of the line $(q+\delta)^2/(1+\delta^2)$, where δ is the normalized detuning from resonance; U. Fano, Phys. Rev. **124**, 1866 (1961).
[18] K. L. Fuchs and R. Kliewer, Phys. Rev. B **3**, 2270 (1971).